

## Article

# Discovery of Stishovite in the Prismatic-Bearing Granulite from Waldheim, Germany: A Possible Role of Supercritical Fluids of Ultrahigh-Pressure Origin

Rainer Thomas <sup>1,\*</sup> , Paul Davidson <sup>2</sup> , Adolf Rericha <sup>3</sup> and Ulrich Recknagel <sup>4</sup><sup>1</sup> Im Waldwinkel 8, D-14662 Friesack, Germany<sup>2</sup> Codes, Centre for Ore Deposits and Earth Sciences, University of Tasmania, Hobart 7001, Australia; paul.davidson@utas.au<sup>3</sup> Alemannenstraße 4a, D-144612 Falkensee, Germany; ruth.rericha@gmx.de<sup>4</sup> Böhmerwaldstraße 22, D-86529 Schrobenhausen, Germany; recknagel-sob@t-online.de

\* Correspondence: rainerthomas@t-online.de

**Abstract:** For the first time in the sixty years since the synthesis of stishovite, we report unambiguous evidence of stishovite formed in the deep Earth. A minimum pressure of about 7.5 GPa at 1000 °C is necessary for the formation of stishovite, corresponding to a depth of about 230 km. In this manuscript we report the identification of stishovite along with coesite as inclusions in mineral grains from the Waldheim granulite. This implies that the stishovite was transported upwards, probably very rapidly to a depth of about 130 km, corresponding to the highest pressure indicated by newly identified coesite in the prismatic of the Waldheim granulite, and continuing up to the depth of emplacement of the Waldheim prismatic granulite. The analysis of the Raman spectra obtained from a metastable trapped stishovite micro-crystal show that all the diagnostic Raman bands are present. However, given the metastability of the stishovite at room temperatures and pressures, this mineral breaks down step-by-step into stable polymorphs, first coesite and then quartz and cristobalite, during the Raman stimulation. The rare coesite crystals in prismatic have also resulted from the irreversible transformation from stishovite. Although the Waldheim occurrence may be unique, we suggest that Raman analysis of co-trapped crystals in similar deep-seated rocks, an area of limited previous research, may prove an important innovation in the study of mantle processes.

**Keywords:** stishovite; coesite; blue shift; supercritical fluid; Waldheim prismatic rock



**Citation:** Thomas, R.; Davidson, P.; Rericha, A.; Recknagel, U. Discovery of Stishovite in the Prismatic-Bearing Granulite from Waldheim, Germany: A Possible Role of Supercritical Fluids of Ultrahigh-Pressure Origin. *Geosciences* **2022**, *12*, 196. <https://doi.org/10.3390/geosciences12050196>

Academic Editors: Jesus Martinez-Frias and Antonio Acosta-Vigil

Received: 25 March 2022

Accepted: 30 April 2022

Published: 4 May 2022

**Publisher's Note:** MDPI stays neutral with regard to jurisdictional claims in published maps and institutional affiliations.



**Copyright:** © 2022 by the authors. Licensee MDPI, Basel, Switzerland. This article is an open access article distributed under the terms and conditions of the Creative Commons Attribution (CC BY) license (<https://creativecommons.org/licenses/by/4.0/>).

## 1. Introduction

Stishovite, the tetragonal high-pressure polymorph of SiO<sub>2</sub>, was named by the Russian high-pressure physicist Sergey M. Stishov, who together with Popova first synthesized the mineral in 1961 [1]. This mineral is very rare at the Earth's surface, having only been found in known or suspected meteorite craters. In 1962 this mineral was found by Chao [2] in the Meteor Crater. Later, stishovite was found in an iron meteorite by Holtstam et al. [3]. According to [4] there are only suggestions of naturally occurring stishovite; currently, this mineral has never been directly observed in metamorphic UHP rock. However, there is good circumstantial evidence which suggests that stishovite was initially present: e.g., as pseudomorphs of coesite after stishovite or precursor-stishovite [5,6].

In this short contribution we concentrate on the description of stishovite found included in almandine of the prismatic-bearing granulite rock from Waldheim, Germany. This rock is part of the ultrahigh-temperature Saxon Granulite Massif, Germany. This complex has an area of roughly 575 km<sup>2</sup>. The general profile contains leucogranulites, pyroxene granulites, pyroclastics, and basic ultramafic rocks. The well-known prismatic granulite from Waldheim (prior to 1996 identified as kornerupine [7]) is an horizon only

a few meters thick, together with biotite- and garnet-rich layers (see e.g., [8]). Details of geology, mineralogy, and petrogenesis are given in [9,10].

One aspect of granulite evolution previously not considered by scientists dealing with the genesis of the prismatic-bearing granulite rock from Waldheim is the input of a boron-rich supercritical fluid/melt, entraining high-pressure minerals from very deep, subducted crustal material (see [11]). At surface temperatures and pressures such materials are observed only as remnants, trapped well outside their normal stability field. Such minerals occur mostly as microscopic rods and spheres, or elliptical bodies including zircon with clear indication of reidite, mixtures of diamond and moissanite, coesite after stishovite, and black globules of columbite-type  $\text{TiO}_2$ .

In this paper we focus on the first description of stishovite found in terrestrial material outside the interior of the Earth. Details of the other findings from Waldheim including reidite, diamond, moissanite, and columbite-type- $\text{TiO}_2$  will be presented in subsequent publications. However, some information relating to coesite in prismatic from Waldheim is given for context.

## 2. Method and Sample

### 2.1. Method

Raman spectra were recorded with the EnSpectr Raman microscope RamMics M532 in the spectral range of 80–4000  $\text{cm}^{-1}$  using a 50 mW single mode 532 nm laser, an entrance aperture of 20  $\mu\text{m}$ , a holographic grating of 1800 g/mm, and a spectral resolution of 4–6  $\text{cm}^{-1}$ . Depending on the grain size, we used microscope objectives with magnifications between 3.2 $\times$  and 100 $\times$ . For the 100 $\times$  objective, we used a long-distance LMPLFLN100 $\times$  from Olympus. The laser energy on the sample was continuously adjusted down to 0.02 mW. The position of the Raman bands was controlled before and after each series of measurements of the Si band, using a single crystal chip of semiconductor-grade silicon. The run-to-run repeatability of the line position (from 20 measurements each) was  $\pm 0.3 \text{ cm}^{-1}$  for Si ( $520.4 \pm 0.3 \text{ cm}^{-1}$ ) and  $0.5 \text{ cm}^{-1}$  for diamond ( $1332.3 \pm 0.5 \text{ cm}^{-1}$  over the range 80–2000  $\text{cm}^{-1}$ ), respectively. As diamond-reference we used a water-clear natural diamond crystal. For azimuth-dependent measurements we used a scaled rotating microscope stage.

For the identification of the different mineral phases using Raman micro-spectroscopy we used the data in [12] and the RRUFF database [13].

### 2.2. Sample

During intense study of the granulite-facies prismatic-bearing rock (Figure 1a,b) from Waldheim/Saxony (see [14,15]) we noted almandine crystals full of mineral inclusions and melt inclusions (Figure 1c). Most of these inclusions form homogeneous phases, which are often water-clear. A vapor bubble, a characteristic feature of melt inclusions in crustal rocks, was always completely absent. In such almandine crystals we found one larger, totally homogeneous and water-clear inclusion ( $20.5 \times 9.3 \mu\text{m}$ ) of stishovite (Figure 1d), which was studied with Raman spectroscopy.

In several minerals, specifically prismaticine [ $(\square, \text{Fe}, \text{Mg})(\text{Mg}, \text{Al}, \text{Fe})_5\text{Al}_4\text{Si}_2(\text{Si}, \text{Al})_2(\text{B}, \text{Si}, \text{Al})(\text{O}, \text{OH}, \text{F})_{22}$ ], zircon, corundum [ $\text{Al}_2\text{O}_3$ ], kyanite [ $\text{Al}_2\text{SiO}_5$ ], and sillimanite, the following mineral phases were found as mineral inclusions: muscovite, clinocllore, coesite (only in prismaticine), diamond, moissanite [ $\text{SiC}$ ], garnet, rutile, dravite, kumdykolite [ $\text{Na}(\text{AlSi}_3\text{O}_8)$ ], kokchetavite [ $\text{K}(\text{AlSi}_3\text{O}_8)$ ], cristobalite, tridymite, and quartz, among others. The diameter of such inclusion is typically about 10  $\mu\text{m}$ . In one case coesite (herein coesite-I) formed an approximately  $64 \mu\text{m} \times 45 \mu\text{m} \times 20 \mu\text{m}$  aggregate of small elliptical crystals accidentally co-trapped in prismaticine (see Figure 2). A smaller crystal ( $30 \mu\text{m} \times 25 \mu\text{m}$ ) was present in the same growth zone of the prismaticine sample (herein coesite-II). Generally, coesite had not intergrown with prismaticine, and appeared clearly as a foreign crystal body. Some coesite crystallites in prismaticine show an extremely large blue shift ( $18 \text{ cm}^{-1}$ ) proportional to the laser power. Synthetic coesites, stishovites, or mixtures of both never show such blue shift. In contrast to stishovite, coesite in prismaticine in our samples was not com-

pletely encapsulated. Therefore, a concurrent formation together with prismaticine cannot be excluded.

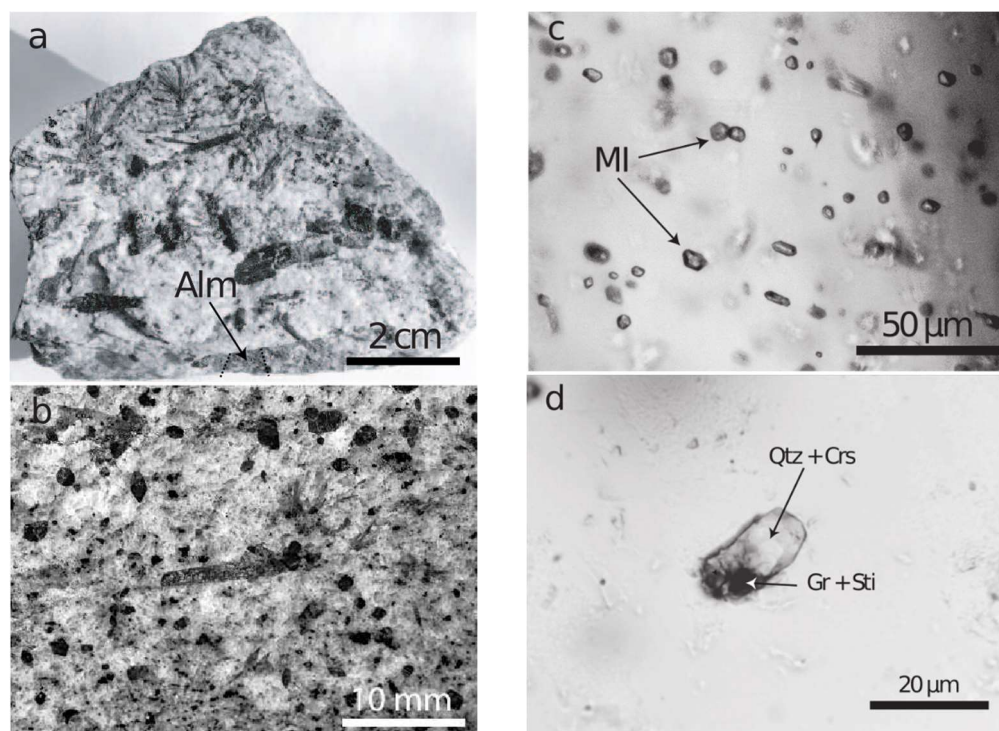


**Figure 1.** Hand specimen (a) of a prismaticine-bearing granulite from Waldheim/Saxony. All dark grains are prismaticine crystals. Alm—almandine. (b) Prismaticine-bearing granulite. In the center, a needle-shaped prismaticine crystal beside more euhedral or subhedral dark grains of prismaticine in a granulite matrix. (c) Melt inclusions in almandine. (d) Melt inclusion in almandine after the first Raman measurement: Crs—cristobalite, Gr—graphite, Qtz—quartz, Sti—remnants of stishovite.

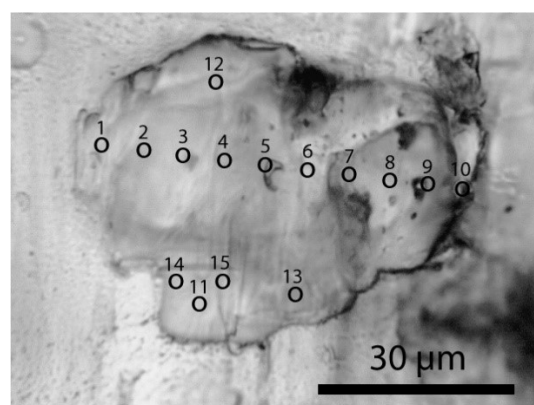


**Figure 2.** Aggregate of coesite-I in prismaticine from the Waldheim/Saxon Granulite Massif. Points 1–15 mark the points of the Raman measurements. Note that between coesite and prismaticine there is a partial thin layer of clinocllore.

For comparison purposes we used stishovite and coesite crystals synthesized at 9 GPa and 900–1000 °C, courtesy of Monika Koch-Müller (GFZ Potsdam). In this connection it is important to emphasize the difference between coesite grown in the coesite pressure and temperature field and that in the stishovite field. According to [16] both fields in the SiO<sub>2</sub>-system are separated by the transition boundary between coesite and stishovite, defined by the linear equation  $P(\text{GPa}) = 4.7 + 0.0031 \times T(\text{K})$ . In the Raman spectrum of coesite formed in the coesite pressure and temperature field, the  $\sim 960 \text{ cm}^{-1}$  band is

completely missing. Coesite from the stishovite field frequently shows this band, which was present in our stishovite sample and in the synthetic stishovite-coesite crystals (Figure 3).

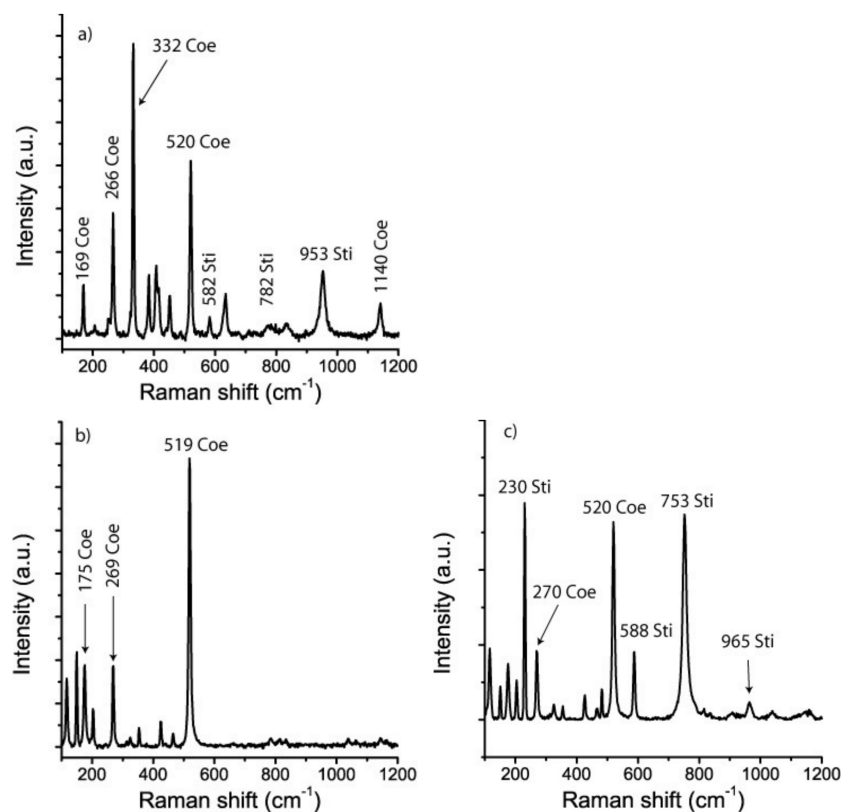


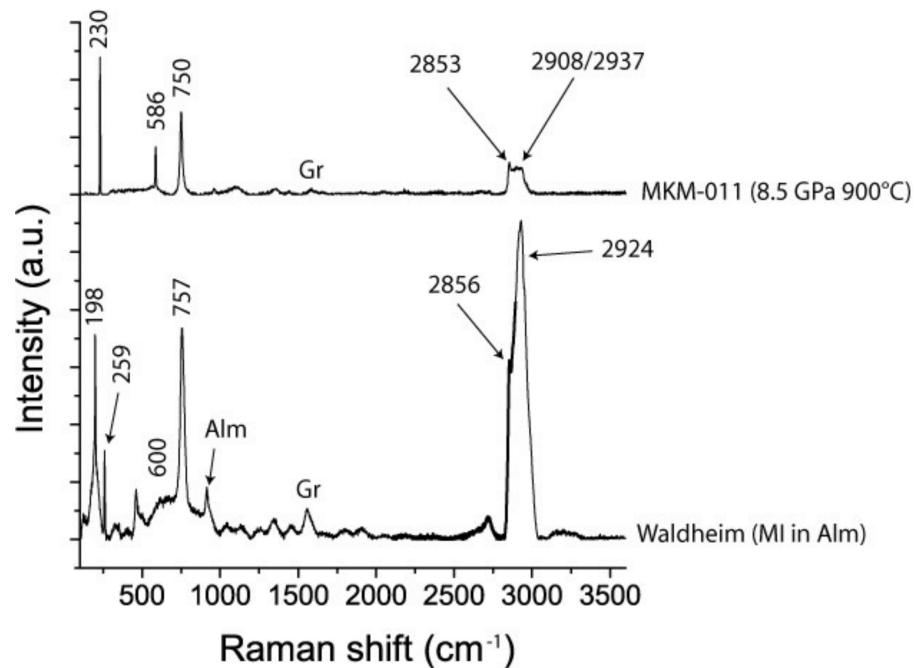
**Figure 3.** Raman spectra of the Waldheim coesite (a) together with synthetic coesite from the coesite and coesite-stishovite fields (b,c). Coe—coesite, Sti—stishovite.

### 3. Results

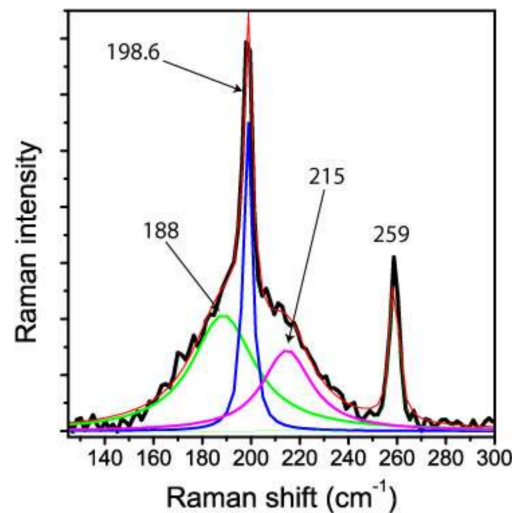
The initial measurements gave an unusual Raman spectrum (see Figure 4) with extremely high intensities in the fingerprint range, and in the OH stretching region beyond 2500 cm<sup>-1</sup> (excited spectrum). The signal of the host mineral almandine was nearly completely suppressed. All “excited” bands can be assigned to stishovite (see [17–20]).

Figure 4 shows the first Raman spectrum obtained, and the assignment, together with the spectrum of a synthetic stishovite crystal. The strong band in the OH stretching region is conspicuous. Nisir et al. [19] found 3.2% H<sub>2</sub>O in water-rich and Al-free stishovite. The water concentration of the natural stishovite in the current study was significantly higher than that value. Using data obtained from the MKM-011 sample, an estimation of the water content gives a value of 8.5% and corresponds to the data presented in [20]. Therefore, the inclusion system with stishovite is more susceptible to laser heating, and graphite dust in the inclusion reinforces this effect.

Figure 5 gives some details of the  $\nu_1$  mode (198.6 cm<sup>-1</sup>). Figure 6 shows the Raman spectrum taken at the same point after laser-induced relaxation of the metastable high-pressure state of stishovite. Certain Raman lines (e.g., the B<sub>1g</sub>-mode) in the primary spectrum represent the frequencies of stishovite corresponding to high pressure (>17.8 up to 52 GPa) generated by local heating of the stishovite inclusion in the rigid garnet host. We assume that the buildup and the following relaxation was triggered by the energy of the laser beam, and was a type of photoinduced, or laser-induced phase transition (see e.g., [21]). The excited state was followed by the total collapse of the stishovite lattice.



**Figure 4.** The Raman spectrum below represents natural stishovite inclusion in almandine after the first measurement. The bands in the fingerprint region, 198, 259, 600, 757  $\text{cm}^{-1}$ , represent the Raman active modes  $\nu_1$  (196),  $B_{1g}$  (235),  $E_g$  (592), and  $A_{1g}$  (754)  $\text{cm}^{-1}$ , respectively. The positions of the very strong bands in the OH stretching region correspond very well to the OH-bands discussed by [19]. The Raman spectrum above is from a synthetic stishovite crystal (sample MKM-011 (8.5 GPa, 900 °C) from Monika Koch-Müller (GFZ Potsdam), given for comparison. Both spectra were taken with the same Raman spectrometer under identical conditions. Alm—almandine, Gr—graphite.



**Figure 5.** Raman spectrum of hydrous stishovite around the  $\nu_1$  band from the first measurement. The broadening of this band in the lower part of Figure 4 can be traced back to frozen components at higher pressure. According [17], the band at 188  $\text{cm}^{-1}$  corresponds to a pressure of 46.9 GPa, and the component at 215  $\text{cm}^{-1}$  to a pressure of 17.8 GPa. The large values for the Full Width at Half Maximum (FWHM) of 58 and 22  $\text{cm}^{-1}$ , respectively, reflect the strong anisotropic behavior of this stishovite mode under pressure, and show that the frozen state does not represent a sharp, single event.

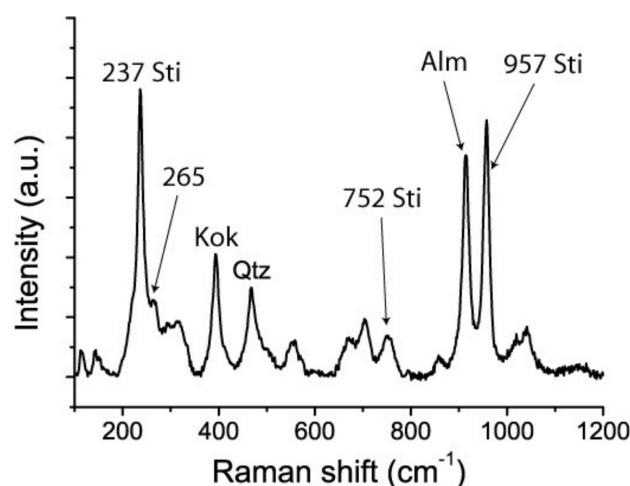


**Figure 6.** Raman spectrum taken from the same point as Figure 1 (lower). The  $\nu_1$  band at  $198\text{ cm}^{-1}$  has disappeared completely, and the  $B_{1g}$  mode of stishovite dominates the spectrum. An additional  $B_{2g}$  mode appears at  $957\text{ cm}^{-1}$ . The  $A_{1g}$  mode is noticeably reduced. Supplementary to the remnants of stishovite appear bands of kokchetavite, quartz, and now the strongest almandine band at  $915\text{ cm}^{-1}$ . The weak or medium band at  $265\text{ cm}^{-1}$  resulted from the release of Al out of the primary stishovite lattice. Alm—almandine, Kok—kokchetavite, Qtz—quartz.

Repetition at the same point gave a completely different Raman spectrum (Figure 6). Instead of the “excited” primary spectrum we found dominant Raman bands of almandine, the strong  $B_{1g}$  mode at  $237\text{ cm}^{-1}$  and the strong  $B_{2g}$  mode at  $957\text{ cm}^{-1}$ , as well as some remnants of stishovite. A third measurement in the surroundings of the first point result identified cristobalite and quartz as products of the breakdown. The stishovite bands had completely disappeared. In addition to cristobalite and quartz we observed the formation of dispersed graphite, perceptible by the D1 and G bands of graphite, in the vicinity of the laser spot.

However, in similar but very rare inclusions in almandine we generally found only two stishovite bands in addition to the breakdown products cristobalite, quartz, and sometimes also kokchetavite. Two lines alone are not enough for unambiguous identification as stishovite.

Coesite was identified by the following characteristic lines (ten measurements each):  $520.2 \pm 5.5$ ,  $331 \pm 5.6$ ,  $265.7 \pm 5.6$ ,  $168.3 \pm 5.6$ , and  $1140.0 \pm 5.6\text{ cm}^{-1}$ . The intensity, the intensity ratio, and also the position of the Raman bands depend strongly on the crystallographic orientation. Table 1 gives the Raman results of different points in coesite-I shown in Figure 2. The numbers leveled with a and b represent data taken using 28 mW and 5 mW, respectively. In this table are also listed some minerals which emerged from the coesite disintegration by the laser irradiation. The steady presence of the  $951.7 \pm 5.4\text{ cm}^{-1}$  band may suggest stishovite-coesite transformation. However, according to the high intensity of this band (not typical for stishovite and coesite) it may represent isolated  $\text{SiO}_4$  tetrahedra [ $\nu_3(\text{T}_2)$ ] (see [22]) formed by the transition of stishovite into coesite. The large blue shift (clearly shown in Figure 7) of all coesite bands (up to  $18\text{ cm}^{-1}$ ) in the coesite crystals may result from strain produced by the lattice mismatch of coesite with remnants of stishovite, indicated by Raman bands at ( $B_{2g}$ )  $952.3 \pm 4.8$ , ( $A_{1g}$ )  $770.9 \pm 4.4$ , ( $E_g$ )  $582.9 \pm 5.0$ , ( $B_{1g}$ )  $206.9 \pm 5.2$ . The blue and red shifts of the  $A_{1g}$  and  $B_{1g}$  modes, respectively, correspond to the higher primary trapping pressure ( $\sim 10\text{ GPa}$ ). We interpret the highly metastable coesite to be a result of the irreversible transformation of the primary stishovite into metastable coesite and further into cristobalite, kokchetavite, corundum and quartz in a completely foreign P-T surrounding. Stishovite formed at greater depth and transported to a higher level has high internal excess energy. An already low addition of energy leads to irreversible signs of decay. Therefore, the Raman measurements are not

exactly reproducible. In the case of coesite-II the disintegration was complete after the first measurement.

**Table 1.** Raman bands of coesite-I in prismatic from Waldheim. Besides the coesite bands, some bands can be assigned to quartz, cristobalite, kokchetavite, and corundum. Numbers in the first column levelled with a and b represent data taken using 28 mW and 5 mW, respectively. These different laser energies are responsible for the generally observed blue shift of the Raman bands in the Waldheim coesite. Note that such a blue shift was never observed in synthetic stishovite or coesite.

Nr.	Coesite						$\alpha$ -Quartz	Cristobalite			Kokchetavite		Corundum		$[\nu_3(\text{T}_2)]$
1a	76.1	175.8	273.1	339.2	527.4	1147.0	458.3	213.5	416.8	784.2	398.9	840.1	-	-	959.2
1b	69.3	167.5	267.6	332.3	521.3	1141.1	453.7	-	414.7	-	382.1	838.4	382.1	632.9	953.2
2a	-	176.1	273.1	339.3	527.3	1146.6	458.3	218.0	416.0	781.1	389.9	826.8	-	-	958.7
2b	69.3	169.2	267.6	332.3	521.3	1141.1	452.1	-	416.5	-	-	-	383.7	634.5	954.7
3a	-	175.9	273.2	339.4	527.4	1146.8	458.3	214.8	415.8	786.7	389.9	843.5	-	-	959.0
3b	-	170.8	267.6	332.3	521.3	1141.1	452.1	-	417.5	-	-	836.7	383.7	636.0	953.2
4a	84.4	175.8	273.1	339.3	527.5	1147.2	447.0	-	416.4	787.6	390.0	840.9	-	639.9	959.0
4b	-	169.2	267.6	333.9	521.3	1142.6	452.1	-	417.5	-	-	-	383.7	634.5	954.7
5a	-	175.7	273.1	339.2	527.3	1146.2	458.4	211.7	416.8	787.8	390.0	840.0	390.0	639.8	958.5
5b	-	166.4	264.8	329.6	518.5	1130.8	449.3	-	414.7	-	-	832.7	380.9	633.2	951.9
6a	76.6	175.9	273.5	339.6	527.6	1147.0	458.7	-	414.1	787.1	390.4	839.9	-	640.2	958.9
6b	-	169.2	267.6	333.9	521.3	1139.7	452.1	-	416.5	-	-	835.7	383.7	634.5	953.2
7a	76.2	176.3	273.5	339.6	527.7	1147.6	458.6	213.8	422.8	782.9	390.2	840.5	-	639.8	959.4
7b	-	-	267.6	333.6	522.0	1141.3	463.2	-	416.0	-	-	-	384.7	635.3	953.4
8a	76.0	176.6	273.3	339.5	527.6	1147.4	458.6	212.4	422.9	779.6	390.1	841.3	-	639.3	959.6
8b	-	167.0	264.8	330.7	519.0	1138.0	450.2	-	416.2	-	-	832.0	381.7	631.8	950.5
9a	76.0	176.4	273.8	339.8	527.9	1147.4	458.8	213.5	414.3	782.4	390.5	839.6	-	640.6	969.7
9b	-	170.5	267.5	333.7	522.1	1144.6	452.9	-	416.5	-	-	836.4	384.3	634.9	953.8
10a	76.0	176.4	273.8	339.8	527.9	1147.4	458.8	213.5	414.3	782.4	390.5	839.6	-	640.6	959.7
10b	72.0	171.2	258.3	335.0	523.2	1143.5	451.5	-	-	-	-	-	386.4	-	957.7
11a	76.0	176.0	271.5	339.5	527.7	1147.7	-	213.8	414.3	-	386.2	-	386.2	-	963.3
11b	69.7	-	260.7	332.7	521.0	1144.1	455.7	-	414.3	-	-	830.5	383.4	-	952.5
12a	78.3	176.8	273.8	340.0	528.2	1147.9	459.0	214.1	414.4	781.6	390.5	841.2	-	641.0	960.2
12b	71.6	169.5	266.2	332.6	521.5	1141.2	452.3	-	416.2	-	-	836.4	382.4	634.7	951.9
13a	75.0	174.4	271.9	338.0	526.1	1145.7	457.5	211.7	412.2	793.6	388.5	835.3	388.5	638.3	957.8
13b	68.0	166.3	265.7	331.4	519.7	1139.6	447.9	-	412.3	-	-	-	382.5	633.3	952.1
14a	75.5	175.8	273.0	339.5	527.5	1147.2	455.5	213.8	413.8	791.8	389.9	833.3	-	640.0	958.4
15a	71.6	-	270.3	336.8	525.1	-	460.6	210.8	418.3	-	389.9	-	378.5	-	952.5

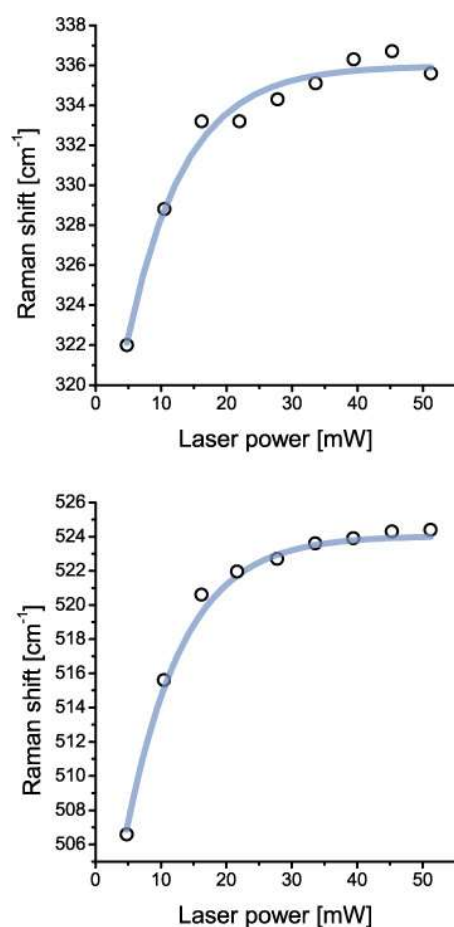


**Figure 7.** Boltzmann sigmoidal fit of the blue shift of prominent coesite bands at 330 and 520  $\text{cm}^{-1}$  independent of laser excitation (532 nm). The significant blue shift ( $\sim 18 \text{ cm}^{-1}$ ) results from the strain generated by the lattice mismatch between primary stishovite (now only remnants) and the resulting coesite. The amount of the blue shift is quasi-reversible due to the blue shift decline over time signaling the destruction of the metastable coesite lattice. Note that no synthetic coesite, stishovite, or mix of those mineral phases, shows such a blue shift.

#### 4. Discussion

According to [4] the “presence of stishovite in subducted crustal rock has been inferred, but as of yet it has not been directly observed (see to this also [23,24]). The rate of obduction of such rocks may not be high enough to permit conservation of stishovite”. While that may be true, it may nevertheless permit the accidental metastable trapping of stishovite as inclusion in a solid stable mineral, here the almandine-rich garnet. The host crystal acts as a “pressure vessel” to prevent inversion of the stishovite to low-pressure polymorphs. The same is also true for other high-pressure minerals such as zircon-reidite, and rutile-columbite-type  $\text{TiO}_2$ .

All lines of the primary Raman spectrum are assignable to hydrous stishovite, in part under high pressure. According to [19] hydrous stishovite after decompression shows a strong and sharp peak  $\nu_1$  at  $196 \text{ cm}^{-1}$  and a peak at  $235 \text{ cm}^{-1}$  corresponding to the  $B_{1g}$  mode. Even the positions of the OH-bands fit very well to the bands at the OH stretching region presented by [19]—see Figure 4 in there.

One Raman band remains problematic: the very sharp band at  $258.7 \text{ cm}^{-1}$ . At standard pressure conditions pure stishovite shows a sharp band at  $235 \text{ cm}^{-1}$  [19]. However, Tschauner [4] pointed out that stishovite at pressures above 30 GPa can accommodate large amounts of Al and  $\text{H}_2\text{O}$  by coupled substitution (see also Lakshtanov et al., 2007 [25]), “whereas at low pressure stishovite does not accommodate other elements beyond trace level”. Therefore, we provisionally assigned this band to the  $B_{1g}$  mode for stishovite with

higher Al- and H<sub>2</sub>O concentration, because the bands in the OH-stretching region also represent an excited state. However, it is also conceivable that this band resulted from the embryonic formation of coesite. The appearance of kokchetavite [K(AlSi<sub>3</sub>O<sub>8</sub>)] after the breakdown of stishovite during the Raman measurement is further evidence that in the primary stishovite a higher Al content is highly possible.

Given all the information obtainable from our Raman measurements, we propose that this is a positive identification of stishovite, albeit in a form that is subject to inversion under laser excitation. It is also possible that other minerals identified in these inclusions may represent partial decrepitation of the host crystals, having permitted inversion due to decompression at some point before or after emplacement.

However, there remains the question of how the stishovite reached its current position. All observation from the geology clearly suggests that this mineral is completely out of place at its current level. Neither of the high-pressure minerals (ultrahydrous stishovite and the water-rich coesite) fit into the accepted genesis model given in [9,10].

An answer may come from the observation of completely rounded (elliptical, spherical) crystals of zircon, corundum, quartz, garnet, and kyanite, among many others, as inclusions in different minerals (see Figure 8). Kalkowsky [26] described tiny, very smooth droplet-like zircon crystals in the prismatic rock, although he did not give any interpretation. No subsequent authors have dealt with this occurrence within the Waldheim granulite.

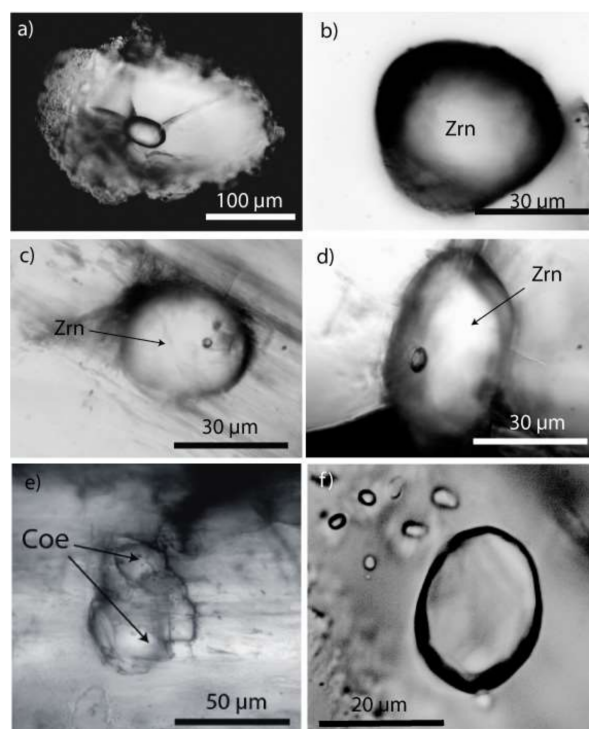


**Figure 8.** Examples of spherical crystals in different minerals from the Waldheim granulite: (a) zircon inclusion in the center of an elliptical high-quartz crystal. The quartz host displays radial fractures due to the volume expansion of the primary reidite-to-zircon transition [27]. (b–d) spherical zircon crystals in prismatic. (e) a conglomerate of coesite ellipsoids in prismatic. There is a thin layer of muscovite and clinocllore between the coesite and the prismatic host. (f) spherical anorthite crystals in an ellipsoidal corundum crystal.

We interpret these spherical, generally single crystals as remnants of crystals initially suspended in a boron-bearing supercritical fluid. From its ultra-deep source, this fluid moved rapidly into the granulite region. Here at a shallower level, the supercritical fluid transformed into a metasomatic-like fluid. The primary mineral load of this fluid was then integrated into the fast-growing crystals (e.g., in almandine and prismatic). Some water-clear dravite crystals contain elliptical kyanite crystals and nanodiamond-bearing

graphite globules beside water-rich silicate melt inclusions (atypical for granulite-facial minerals)—see Figure 9. In some ways, this mechanism resembles the idea (pegmatitic metatect) described in [28]. According to our observations, however, the origin of this fluid is very different.

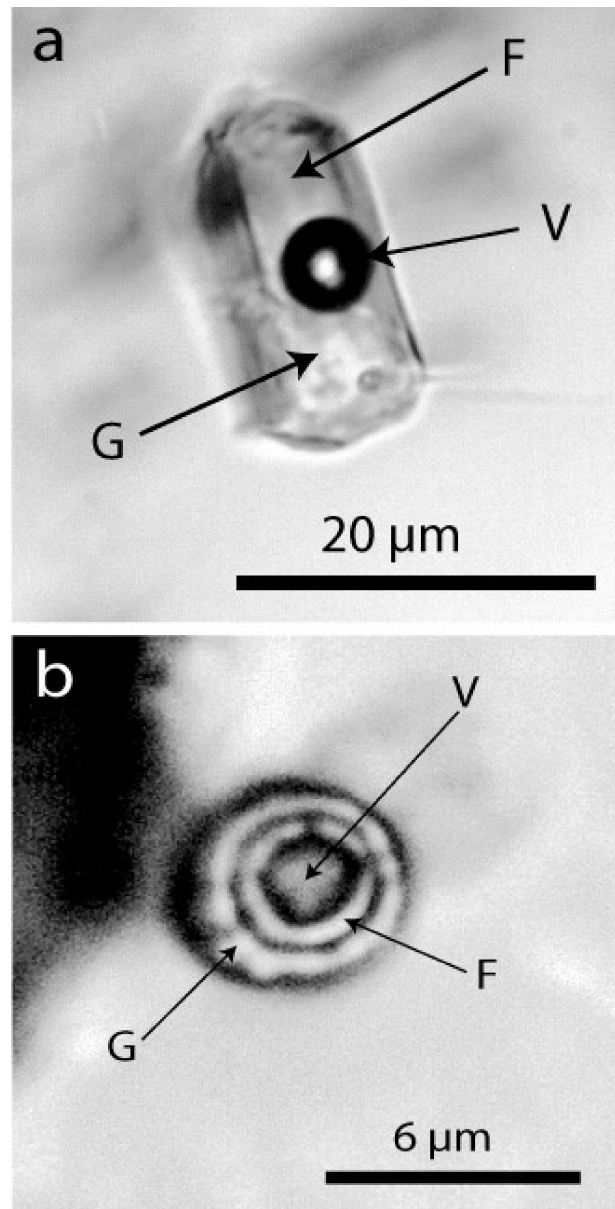


**Figure 9.** Water-rich melt inclusions in dravite. The inclusion (a) represents a typical volatile-rich melt inclusion, and (b) is a supercritical melt inclusion (see [29]). F—water-rich fluid phase, G—glass (often partially crystallized), V—vapor phase.

Some larger elliptical crystals contain smaller spherical crystals or melt inclusions. Some are very exotic, e.g., hexahydrite  $[\text{MgSO}_4 \cdot 6\text{H}_2\text{O}]$ , among simple sulfates and others. In the associated processes, minerals such as stishovite and coesite were trapped in a metastable state in the surrounding, growing host crystals. An analogy here might be the rapid migration of kimberlite magma to the surface, where crystal fragments become rounded during the fast transport (see here [30]), and diamonds preserved from complete inversion to graphite. Graphite pseudomorphs after diamond have often been found in high-grade metamorphics (see e.g., [5]).

Furthermore, our results shed light on the problem of laser power used for the study of small inclusions in a matrix. Local volume expansion by laser heating of a small inclusion in a rigid host can increase pressure to extreme values, which can result in a red or blue shift of Raman lines, depending on the pressure/temperature-dependence of Raman mode frequencies. Another example is the presence of graphite, as the inclusion can be locally heated to values such that small nanocrystals of diamond are rapidly inverted to graphite. Furthermore, the disintegration of the metastable states of a mineral, generated by insertion of elements (e.g., Al) at high pressure, can be triggered by excessive laser power; we observed this in the inversion of Al-rich coesite into corundum and other daughter products. The high H<sub>2</sub>O (about 4000 ppm) and Al content are indications that the coesite was initially formed at very high pressure. Information regarding the water measurements will be presented in a forthcoming paper.

From the metastability of high-pressure mineral phases, we suggest that it is necessary to start Raman investigations on minerals and mineral inclusions at low laser power (~5 mW on the sample). According to Kaminsky (oral communication), this is also relevant for X-ray analyses of stishovite using ESRF synchrotron facilities.

## 5. Conclusions

In summary, we propose a multi-stage model to explain the presence of stishovite inclusions in granulite rock apparently formed at much lower temperatures and pressures than the stishovite stability field. At pressures greater than 3 GPa, studies ([31,32] have shown that H<sub>2</sub>O and aluminosilicate melts are completely miscible in any proportion, and the resulting melt/fluids have extremely low density, and viscosities approaching those water or honey at room temperatures. Previously we have referred to these as supercritical melt/fluids, since they have exceptional properties, and below a critical temperature and pressure dissociate into conjugate H<sub>2</sub>O- and aluminosilicate-rich phases (see [29,33]). We propose that such fluids forming within the stishovite stability field would be rapidly expelled and forced upwards, in the process entraining small crystals of very high-pressure minerals, including stishovite. This transport is, of necessity, rapid, due to the minerals' enormous density and viscosity in contrast with their deep-crustal hosts. Any entrained grains would tend to be rounded by attrition, and possibly some corrosion during transport out of their stability fields. However, such grains may also be subject to accidental co-trapping in crystals growing in the ascending supercritical melt/fluid. Upon reaching the coesite stability field, grains of that phase may also be entrained or may grow in the ascending fluid. Given the presence of prismaticite it is possible that these fluids are boron-rich. Minerals with stability fields greater than coesite may be found completely enclosed in a host mineral, while coesite was occasionally found embedded, but not completely enclosed, in prismaticite. This may suggest co-crystallization of prismaticite and coesite, possibly indicating some constraints on temperatures and pressures at that point. The survival well outside their stability fields of extremely high-pressure phases such as stishovite, coesite, reidite, diamond, moissanite, and others, is only possible if the abraded grains are trapped as inclusions within another mineral that can act as a "pressure vessel". However, such grains are inherently metastable, and tend to relaxation by energy input (laser energy) and force an inversion to their low-pressure stable analogues. Decrepitation of the host crystal is often the cause of such volume changes, and the numerous examples of grains showing partial or complete inversion, such as those combining stishovite–quartz or zircon–reidite, testifies to this. Equally, the burst of energy applied by laser during Laser Raman Analysis can have the same effect, but the process of inversion takes a finite amount of time, and we have shown the successive stages of the process over three successive analyses of the same crystal inclusion. We propose that the final step was the injection of a supercritical melt/fluid, possibly as a dike swarm, into the granulite facies assemblage at Waldheim, with the subsequent formation of the prismaticite granulite. Thus, while the host rocks indicate no more than granulite facies temperatures and pressures, their minerals

may contain co-trapped crystals from a much deeper source with higher temperatures and pressures.

## 6. Outlook

The present study of the prismatic-bearing granulite rock from Waldheim throws light on the multistage formation of a high-pressure and high-temperature complex with many unusual minerals. With sophisticated studies we can expect further findings of minerals of type B, Si- and Fe-carbides, or their mixtures. So, our measurements open a window for investigations in future.

**Author Contributions:** R.T., P.D., A.R. and U.R. designed the project; R.T. performed the Raman analyses; all authors contributed to the interpretation and did comprehensive editing and have read and agreed to the published version of the manuscript. All authors have read and agreed to the published version of the manuscript.

**Funding:** This research received no external funding.

**Institutional Review Board Statement:** Not applicable.

**Informed Consent Statement:** Not applicable.

**Data Availability Statement:** Not applicable.

**Acknowledgments:** Monika Koch-Müller (GFZ Potsdam) is thanked for some synthetic coesite and stishovite crystals for comparison and measurements, and Edward Grew is thanked for intense discussion. Finally, we thank the contributions and comments from two anonymous reviewers, and Felix V. Kaminsky.

**Conflicts of Interest:** The authors declare no conflict of interest.

## References

1. Stishov, S.M.; Popova, S.V. New dense polymorphic modification of silica (in Russian). *Geokhimiya* **1961**, *10*, 837–839.
2. Chao, E.C.T.; Fahey, J.J.; Littler, J.; Milton, D.J. Stishovite, SiO<sub>2</sub>, a very high pressure new mineral from Meteor Crater, Arizona. *J. Geophys. Res. Earth Surf.* **1962**, *67*, 419–421. [[CrossRef](#)]
3. Holtstam, D.; Broman, C.; Söderhielm, J.; Zetterqvist, A. First discovery of stishovite in an iron meteorite. *Meteorit. Planet. Sci.* **2003**, *38*, 1579–1583. [[CrossRef](#)]
4. Tschauner, O. High-pressure minerals. *Am. Miner.* **2019**, *104*, 1701–1731. [[CrossRef](#)]
5. Dobrzhinetskaya, L.F.; Faryad, S.W. Frontiers of Ultrahigh-Pressure Metamorphism: View from Field and Laboratory. In *Ultrahigh-Pressure Metamorphism 25 Years After the Discovery of Coesite and Diamond*; Chapter 1; Dobrzhinetskaya, L.F., Faryad, S.W., Wallis, S., Cuthbert, S., Eds.; Elsevier: Amsterdam, The Netherlands, 2011; pp. 1–39.
6. Kaminsky, F. Mineralogy of the lower mantle: A review of ‘super-deep’ mineral inclusions in diamond. *Earth-Sci. Rev.* **2012**, *110*, 127–147. [[CrossRef](#)]
7. Grew, E.S.; Cooper, M.A.; Hawthorne, F.C. Prismatic: Revalidation for boron-rich compositions in the kornerupine group. *Miner. Mag.* **1996**, *60*, 483–491. [[CrossRef](#)]
8. Werner, C.-D. *Saxonian Granulites—Igneous or Lithogenous. A Contribution to the Geochemical Diagnosis of the Original Rocks in High-Metamorphic Complexes*; ZfI-Mitteilungen: Leipzig, Germany, 1987; pp. 221–250.
9. Rötzler, J.; Hagen, B.; Hoernes, S. Geothermometry of the ultrahigh-temperature Saxon granulites revisited. Part I: New evidence from key mineral assemblages and reaction textures. *Eur. J. Miner.* **2008**, *20*, 1097–1115. [[CrossRef](#)]
10. Hagen, B.; Hoernes, S.R. Geothermometry of the ultrahigh-temperature Saxon granulites revisited. Part II: Thermal peak conditions and cooling rates inferred from oxygen-isotope fractionations. *Eur. J. Miner.* **2008**, *20*, 1117–1133. [[CrossRef](#)]
11. Zagorsky, V.Y. Deep fluid flow–melt interaction and problems of granite–pegmatite system petrogenesis. Abstracts in Granitic pegmatites: The state of the art. *Memórias Porto* **2007**, *8*, 106–107.
12. Hurai, V.; Huraiova, M.; Slobodnik, M.; Thomas, R. *Geofluids—Developments in Microthermometry, Spectroscopy, Thermodynamics, and Stable Isotopes*; Elsevier: Amsterdam, The Netherlands, 2015; 489p.
13. Lafuente, B.; Downs, R.T.; Yang, H.; Stone, N. The power of databases: The RRUFF project. In *Highlights in Mineralogical Crystallography*; Armbruster, T., Danisi, R.M., Eds.; De Gruyter: Berlin, Germany; München, Germany; Boston, MA, USA, 2016; pp. 1–30. ISBN 9783110417104.
14. Grew, E.S. A second occurrence of Kornerupine in Waldheim, Saxony, German Democratic Republic. *Z. Geol. Wiss.* **1989**, *17*, 67–76.
15. Thomas, R.; Grew, E. *Coesite Inclusions in Prismatic from Waldheim, Germany: New Constraints on the Pressure-Temperature Evolution of the Saxony Granulite Complex*; Book of Abstracts, 3rd European Mineralogical Conference; EMC: Cracow, Poland, 2021; p. 391.

16. Ono, S.; Kikegawa, T.; Higo, Y.; Tange, Y. Precise determination of the phase boundary between coesite and stishovite in SiO. *Phys. Earth Planet. Inter.* **2017**, *264*, 1–6. [[CrossRef](#)]
17. Hemley, R.J. Pressure dependence of Raman spectra of SiO<sub>2</sub> polymorphs: A-quartz, coesite, and stishovite. In *High-Pressure Research in Mineral Physics*; Manghnani, M.H., Syona, Y., Eds.; Terra Scientific Publishing Company (TERRAPUB): Tokyo, Japan; American Geophysical Union: Washington, DC, USA, 1987; pp. 347–359.
18. Hemley, R.J.; Mao, H.-K.; Chao, E.C.T. Raman spectrum of natural and synthetic stishovite. *Phys. Chem. Miner.* **1986**, *13*, 285–290. [[CrossRef](#)]
19. Nisr, C.; Shim, S.-H.; Leinenweber, K.; Chizmeshya, A. Raman spectroscopy of water-rich stishovite and dense high-pressure silica up to 55 GPa. *Am. Miner.* **2017**, *102*, 2180–2189. [[CrossRef](#)]
20. Lin, Y.; Hu, Q.; Meng, Y.; Walter, M.; Mao, H.-K. Evidence for the stability of ultrahydrous stishovite in Earth's lower mantle. *Proc. Natl. Acad. Sci. USA* **2019**, *117*, 184–189. [[CrossRef](#)] [[PubMed](#)]
21. Zong, A.; Kogar, A.; Bie, Y.-Q.; Rohwer, T.; Lee, C.; Baldini, E.; Ergeçen, E.; Yilmaz, M.B.; Freelon, B.; Sie, E.J.; et al. Evidence for topological defects in a photoinduced phase transition. *Nat. Phys.* **2019**, *15*, 27–31. [[CrossRef](#)]
22. Zhai, K.; Xue, W.; Wang, H.; Wu, X.; Zhai, S. Raman spectra of sillimanite, andalusite, and kyanite at various temperatures. *Phys. Chem. Miner.* **2020**, *47*, 23. [[CrossRef](#)]
23. Gisl, P.D.; Dache, F. Effect of Pressure and Temperature on the Reversal Transitions of Stishovite. *Meteoritics* **1968**, *4*, 123–136. [[CrossRef](#)]
24. Hemley, R.J.; Prewitt, C.T.; Kingma, K.J. Chapter high-pressure behavior of silica. *Silica* **1994**, *29*, 41–82. [[CrossRef](#)]
25. Lakshtanov, D.L.; Litasov, K.D.; Sinogeikin, S.V.; Hellwig, H.; Li, J.; Ohtani, E.; Bass, J.D. Effect of Al<sup>3+</sup> and H<sup>+</sup> on the elastic properties of stishovite. *Am. Miner.* **2007**, *92*, 1026–1030. [[CrossRef](#)]
26. Kalkowsky, E. Der Korundgranulit von Waldheim in Sachsen. In *Abhandlungen der Naturwissenschaftlichen Gesellschaft ISIS in Dresden*; Hofbuchhandlung H. Burdach: Dresden, Germany, 1907; Volume 2, pp. 47–65.
27. Thomas, R.; Davidson, P.; Rericha, A. Prismatic granulite from Waldheim/Saxony: Zircon-Reidite. *J. Earth Envi. Sci. JEES-103* **2022**, *1*, 1–3.
28. Scheumann, K.H. Das Kornerupingestein von Waldheim in Seinem Genetischen Zusammenhang. *Abhandlungen der Sächsischen Akademie der Wissenschaften zu Leipzig. Mathematisch-naturwissenschaftliche Klasse* **1960**, *47*, 22.
29. Thomas, R.; Davidson, P.; Rericha, A.; Voznyak, D. Water-Rich Melt Inclusion as “Frozen” Samples of the Supercritical State in Granites and Pegmatites Reveal Extreme Element Enrichment Resulting Under Non-Equilibrium Conditions. *Miner. J.* **2022**, *44*, 3–15. [[CrossRef](#)]
30. Arndt, N.T.; Guitreau, M.; Boullier, A.-M.; Le Roex, A.; Tommasi, A.; Cordier, P.; Sobolev, A. Olivine, and the origin of kimberlite. *J. Petrol.* **2010**, *51*, 573–602. [[CrossRef](#)]
31. Ni, H.; Zhang, L.; Xiong, X.; Mao, Z.; Wang, J. Supercritical fluids at subduction zones: Evidence, formation condition, and physicochemical properties. *Earth-Sci. Rev.* **2017**, *167*, 62–71. [[CrossRef](#)]
32. Manning, C.E. The Influence of Pressure on the Properties and Origins of Hydrous Silicate Liquids in Earth's Interior. In *Magmas Under Pressure*; Chapter 3; Kono, Y., Sanloup, C., Eds.; Elsevier: Amsterdam, The Netherlands, 2018; pp. 83–113.
33. Thomas, R.; Davidson, P.; Appel, K. The enhanced element enrichment in the supercritical states of granite–pegmatite systems. *Acta Geochim.* **2019**, *38*, 335–349. [[CrossRef](#)]